Quasi-steady drift paths in a model magnetosphere with AMIE electric field: Implications for ring current formation

Margaret W. Chen,[1] Michael Schulz,[2] Gang Lu,[3] and Larry R. Lyons[4]

[1]   Recent measurements show that magnetospheric convection electric fields during the main phases of magnetic storms are much more complicated in spatial structure than the electric fields that have generally been used to model formation of the stormtime ring current. To investigate the transport effects of such more realistic stormtime electric fields on magnetospheric charged particles, we map the Assimilative Model of Ionospheric Electrodynamics (AMIE) electric potential functions analytically with a simple magnetic field model at selected times of interest during several magnetic storms from 1997–1998 and during the extremely large storm of July 2000. We calculated corresponding contours of constant Hamiltonian (kinetic plus potential energy) for first invariant values that range from 0 to 30 MeV/G (representative of equatorially mirroring cold plasma, ring current, and radiation-belt ions and electrons). These equatorial contours would constitute drift paths if the electric field were truly constant in time. We thus calculated how far along such quasi-drift paths the corresponding particles would have drifted after specific amounts of time, and we compare these quasi-drift characteristics with those obtained from a simple semiempirical model of the convection electric field. We find considerable variability among stormtime equatorial quasi-drift paths, reflecting the known variability of AMIE equipotentials. Patterns of equatorial quasi-drift in the simplified electric field model are (by construction) symmetric about the dawn-dusk meridian. During the main phases of storms, the equatorial electric field derived from AMIE tends to be strongest in an MLT sector several hours wide on the night side. This concentration of AMIE equipotentials provides a channel for rapid transport (requiring $\sim$20–30 min) for ions with first invariant values representative of the ring current population from the nightside neutral line to low L values ($\sim$3–4) near dusk, where the partial ring current forms. During the extremely large "Bastille Day" storm of 15 July 2000 (minimum $Dst = -300$ nT) the drift patterns derived from AMIE show penetration of ions to as low as $L \sim 2$. This deep penetration of ring current ions could help to account for the very strong ring current that was observed during this storm. The quasi-steady state drift properties help us anticipate the implications of a more realistic electric field model for the particle drifts that lead to the formation of the stormtime ring current.   *INDEX TERMS:* 2730 Magnetospheric Physics: Magnetosphere—inner; 2778 Magnetospheric Physics: Ring current; 2788 Magnetospheric Physics: Storms and substorms; 2712 Magnetospheric Physics: Electric fields (2411); *KEYWORDS:* particle transport, ring current, storms, storm-time electric field, particle drift trajectories

1. Introduction

[2]   The magnetospheric electric field plays a critically important role in the transport of particles within the inner

[1]Space Sciences Applications Laboratory, The Aerospace Corporation, El Segundo, California, USA.
[2]Lockheed Martin Advanced Technology Center, Palo Alto, California, USA.
[3]High Altitude Observatory, Boulder, Colorado, USA.
[4]Department of Atmospheric Sciences, University of California, Los Angeles, Los Angeles, California, USA.

magnetosphere. Electric fields affect particle drift trajectories and drift rates. They thereby determine many important plasma signatures of the inner magnetosphere (e.g., the location of the plasmapause, the circulation of cold plasma within the plasmasphere, and the penetration of the plasma sheet into the inner magnetosphere to form the ring current). Many investigators have used heuristic electric field models derived from an electrostatic potential $\Phi \propto L^{\gamma} \sin \phi$, where ϕ is the magnetic local time and γ is an adjustable index, to trace particle drifts in the inner magnetosphere. The case $\gamma = 1$ [*Nishida*, 1966; *Brice*, 1967] corresponds to an equatorially uniform electric field in the inner magnetosphere and has been used [e.g., *Kavanagh et al.*, 1968; *Chen*, 1970] to

model the penetration of low-energy particles. The case $\gamma = 2$ [*Volland*, 1973, 1975; *Stern*, 1974, 1975] corresponds to a shielded electric field and has been used in several ring current modeling studies [e.g., *Ejiri*, 1978, *Smith et al.*, 1979; *Fok et al.*, 1995; *Jordanova et al.*, 1994; *Ebihara and Ejiri*, 2000]. *Chen et al.* [1993, 1994, 2000] have used a superposition of quiescent shielded (Volland-Stern) and impulsive unshielded (Brice-Nishida) electric fields to trace drift paths of ions that form the stormtime ring current.

[3] Recent CRRES and DMSP satellite measurements [*Wygant et al.*, 1998; *Rowland and Wygant*, 1998; *Anderson et al.*, 2001], along with Millstone Hill radar measurements [*Yeh et al.*, 1991], show that stormtime magnetospheric electric fields are significantly more complicated in spatial structure than the above-mentioned models. We would expect this greater complexity of the stormtime magnetospheric electric field to have significant effects on the inward transport of plasmasheet particles to form the stormtime ring current. However, the cited measurements have been too limited in spatial coverage to provide an improved global magnetospheric electric field model for tracing stormtime particle drifts. Time-averaged semiempirical models [e.g., *Maynard et al.*, 1983; *Weimer*, 1995] dependent on Kp are instructive for orientation but are of limited use for modeling particle drifts during individual magnetic storms. *Kistler and Larson* [2000] and *Jordanova et al.* [2001] have found the IMF-dependent parameterized electric field model of *Weimer* [1996] in a dipole magnetic field to produce ion fluxes in the ring current region that agree better with observations than those produced in the Volland-Stern model for a few storm events. However, the *Weimer* [1996] model has limited statistics for stormtime conditions. We have decided instead to use AMIE, the Assimilative Model of Ionospheric Electrodynamics [*Richmond and Kamide*, 1988], for modeling particle drifts in the present study and for simulating the stormtime ring current in the near future.

[4] AMIE fits ionospheric potentials to electric field data provided by ground-based magnetometers, radars, and satellites. Ground-based magnetometer chains provide fairly good spatial coverage, especially at latitudes above 50°. In situ electric field data may provide better latitudinal coverage but are typically sparse in local-time coverage. Nonetheless, for a given event we expect this assimilative model to provide a more realistic representation of stormtime electric fields than simplified heuristic [*Volland*, 1973, 1975; *Stern*, 1974, 1975; *Maynard and Chen*, 1975] or time-averaged semiempirical models [*Maynard et al.*, 1983; *Weimer*, 1995, 1996] can provide.

[5] In our present study we map AMIE potentials throughout the simple magnetospheric field model [*Dungey*, 1963] obtained by adding a uniform southward field to the Earth's dipole field. Use of this simple magnetic field model allows us to map electric potentials analytically, in contrast (for example) to *Boonsiriseth et al.* [2001], who needed to map potentials numerically because they used the more complicated magnetic field model of *Tsyganenko* [1996]. Here we calculate ion and electron drift trajectories and the elapsed times required to execute them in several "frozen-in-time" realizations of AMIE electric fields obtained during several magnetic storms, including three large storms selected for detailed study by the NSF Geospace Environ-

ment Modeling (GEM) Inner Magnetosphere Storms Campaign and the extremely large "Bastille Day" storm of 15 July 2000.

[6] In other words we allow our representative particles to follow paths of constant kinetic plus potential energy (i.e., contours of constant Hamiltonian) without allowing the electric field to evolve realistically in time through the course of the simulation. This study is therefore only a prelude to the simulation of actual particle drift paths through the time-varying AMIE electric field for a real storm. Our purpose here is to learn about the properties of such contours in order to help us later interpret results of truly time-dependent bounce-averaged guiding-center drift simulations.

[7] Accordingly, we compare the drift characteristics (spatial patterns and times required for their execution) obtained from "frozen-in-time" realizations of AMIE electric fields with those obtained from corresponding "frozen-in-time" realizations of our simple model electric fields derived from superimpositions of shielded (Volland-Stern, $\gamma = 2$) and unshielded (Brice-Nishida, $\gamma = 1$) potential functions. These comparisons help us anticipate the implications of a more realistic electric-field model for the particle drifts that lead to formation of the stormtime ring current.

2. Mapping AMIE Potentials in Analytical Magnetic Field Models

[8] Although commonly displayed as plots, AMIE potentials are in fact based on an analytical expansion in terms of colatitude and magnetic local time ϕ in the ionosphere, so that

$$\Phi_{AMIE}(\theta, \phi, t) \quad = \quad \sum_i a_i(t)\, \Phi_i(\theta, \phi) \qquad (1)$$

where the a_i are AMIE expansion coefficients and t denotes time. The basis functions Φ_i are constructed from associated Legendre functions with nonintegral index n at high latitudes and a linear combination of trignometric functions at low latitudes [*Richmond and Kamide*, 1988]:

$$\Phi_i(\theta, \phi) = K_{1i} P_n^{|m|}(\cos \theta) f_m(\phi) \qquad \theta < \theta_0,\ \theta > \pi - \theta_0$$

$$= K_{2i} [\cot^m(\theta/2) + \tan^m(\theta/2)] f_m(\phi) \quad \theta_0 < \theta < \pi - \theta_0$$

$$(2)$$

$$\begin{aligned} f_m(\phi) &= \sqrt{2} \cos m\phi & m < 0 \\ &= 1 & m = 0 \qquad (3) \\ &= \sqrt{2} \sin m\phi & m < 0. \end{aligned}$$

where θ_0 is the colatitude that is (typically chosen to be 40°) at which the expansions in equation (2) are forced to match smoothly, m is the azimuthal wave number, and K_{1i} and K_{2i} are normalizing constants that cause the gradients of the basis functions to be orthonormal over the ionosphere and continuous at $\theta = \theta_0$. The eigenvalues n are determined by matching logarithmic derivatives of the high- and low-latitude basis functions at $\theta = \theta_0$. AMIE

potentials are not usually calculated equatorward of $\theta = \theta_0$ in practice. The AMIE coefficients a_i are determined via least-squares fit of the analytical expansion (1) to magnetometer data and to any available satellite and radar data.

[9] AMIE potentials can be mapped analytically to anywhere in a magnetic field model in which the field-line label L can be expressed explicitly in terms of the colatitude θ. For this study we use such a magnetic field model, namely that which results from superposition of a dipolar magnetic field and a uniform southward ΔB parallel to the dipole axis [Dungey, 1963]. The resulting field is specified by

$$\mathbf{B}(r, \theta) = \mu_E \nabla \left[(1/r^2) \cos \theta - (r/b^3) \cos \theta \right] \qquad (4)$$

where r is the geocentric distance and b is the radius of the equatorial neutral line. The strength of ΔB is chosen here so that the circular boundary between closed and open field lines intersects the Earth at colatitude $\theta^* = 20°$. In this case the uniform southward ΔB has an intensity of 14.7 nT and leads to $b = 12.82\ R_E$. The equation of a field line in this model is

$$r = La \left[1 + (1/2)(r/b)^3 \right] \sin^2 \theta, \qquad (5)$$

where a is the Earth's radius and L is the dimensionless magnetic-shell label inversely proportional to the amount of magnetic flux enclosed. The label of the last closed field line is thus $L^* = 2b/3a$, so that $L^* = 8.5466$ for $\theta^* = 20°$. According to equation (5), the relationship between L and θ at altitude $r - a = 110$ km is thus

$$L = 1.017/\sin^2 \theta, \qquad (6)$$

and this relationship allows AMIE potentials to be expressed as $\Phi_{AMIE}(L, \phi, t)$, a function of L, ϕ, and t.

[10] This simple magnetic field model preserves essential features of the relevant physical processes, while still letting us simplify the derivation of the particle kinematics in the model. For this study we have kept ΔB and thus the radius of the neutral line constant during the storm. In future studies we plan to change ΔB with time so that the size of our model magnetosphere varies more realistically. A time-varying magnetic field would lead to induced electric fields that we do not explicitly consider in the present study. In the future we also plan to include day-night asymmetry in the magnetic field model.

3. Hamiltonian Function

[11] In the present study we consider only equatorially mirroring particles that conserve their first two invariants M and J (=0) as they drift within the model magnetosphere. Adiabatic drift paths are thus contours of constant M for the Hamiltonian function

$$\begin{aligned} H(L, \phi, t) = \left(2MB_0 m_0 c^2 + m_0^2 c^4 \right)^{1/2} &- m_0 c^2 + q[-V_\Omega/L \\ &+ \Phi_E(L, \phi, t)], \end{aligned} \qquad (7)$$

where B_0 is the equatorial magnetic field value (a function of L), q is the particle charge, V_Ω (= 90 kV) is the corotation

potential at $L = 1$, and Φ_E is the electrostatic convection potential function. In the past we have considered a simple convection potential function

$$\Phi_{simple} = -\frac{V_\Omega}{L} + \frac{V_0}{2} \left(\frac{L}{L^*} \right)^2 \sin \phi + \frac{\Delta V(t)}{2} \left(\frac{L}{L^*} \right) \sin \phi \qquad (8)$$

including a time-independent shielded ($\gamma = 2$) term with $V_0 = 25$ kV and an unshielded ($\gamma = 1$) time-dependent term from which the storm-associated electric field enhancement was derived. Hereafter in this paper we will refer to this as the "simplified" electric field model, for comparison with results obtained by using the AMIE potential Φ_{AMIE} given by equation (1) in the Hamiltonian function specified by equation (7).

[12] In the present study we use the AMIE coefficients obtained for selected times during several magnetic storms as if these coefficients were time-independent, and so we calculate particle drift paths from the Hamiltonian specified by (7) as if the AMIE electric field were time-independent. Moreover, we compare these quasi-steady AMIE drift paths with drift paths obtained from corresponding time-independent realizations of the simplified convection electric potential given by equation (8).

4. Equipotentials

[13] As we have mentioned, AMIE convection electric fields are usually illustrated by plotting their equipotential contours on a spherical surface at altitude 110 km in the ionosphere. Since we are interested here in magnetospheric effects of AMIE electric fields, we illustrate their spatial characteristics by mapping ionospheric AMIE potentials to the equatorial plane. We do this at various representative times during the four magnetic storms of interest: those of 19 October 1998 (minimum $Dst = -112$ nT), 25 September 1998 (minimum $Dst = -207$ nT), 15 May 1997 (minimum $Dst = -115$ nT), and 15 July 2000 (minimum $Dst = -300$ nT). The first three of these storms were those selected for detailed analysis by the NSF GEM Inner Magnetosphere Storms Campaign. The fourth is the famous "Bastille Day" storm, so named for the date of the corresponding coronal mass ejection. AMIE potentials were obtained for these storms by using DMSP drift meter and magnetometer data. The transitional colatitude θ_0 was taken to be at $40°$ in the AMIE runs for these storms. However, DMSP drift meter data for the 19 October 1998 storm indicate significant penetration of the stormtime electric field to roughly $50°$ latitude [Anderson et al., 2001].

[14] Equipotential surfaces of the combined (convection plus corotation) potential function correspond to drift shells of particles with zero kinetic energy. We therefore include the corotation potential in computing all the equipotential patterns plotted in this paper. Figure 1 shows equipotential contours of the combined potential function (corotation plus AMIE convection) in the equatorial plane of our model magnetic field at selected times (prestorm, main phase, and recovery phase) associated with the 19 October 1998 storm. The dotted circle at $b = 12.82\ R_E$ corresponds to the neutral line and thus to the boundary of our model. The dashed circle at 2.47 R_E maps to $50°$ latitude at altitude 110 km in
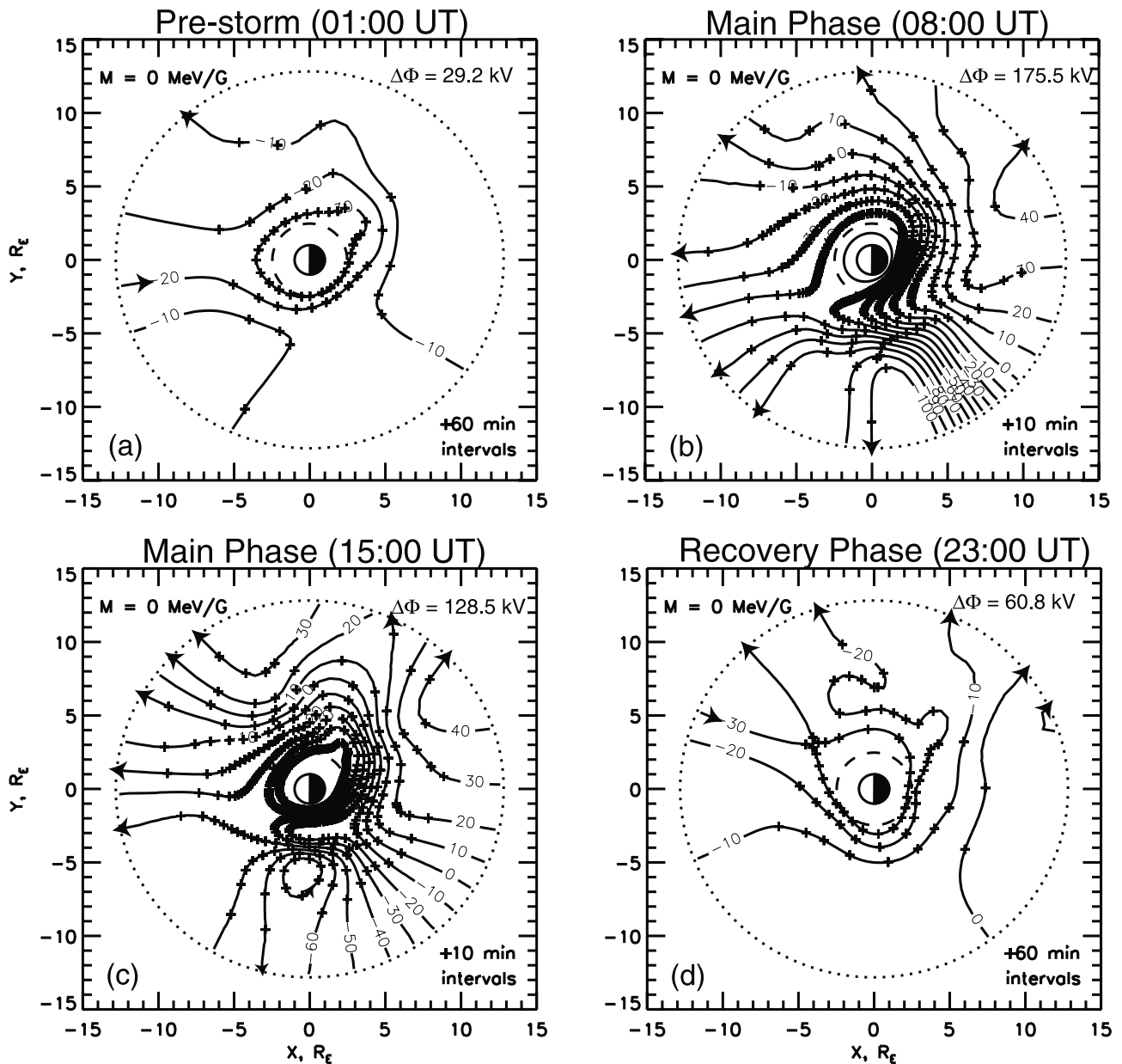
Figure 1. Patterns of equatorial AMIE plus cororation equipotentials are shown for representative times during (a) prestorm (0100 UT), (b) early main phase (0800 UT), (c) recovery phase (1500 UT), and (d) recovery phase (2300 UT) of the 19 October 1998 storm. The black curves are contours of constant Hamiltonian in units of keV per charge. The plus signs mark drift time intervals. The dashed curve at 2.54 R_E maps to the AMIE transitional latitude of 50° in our magnetic field model.

our magnetic field model. The equipotentials are smooth across the transitional latitude $90° - \theta_0$. However, one needs to be cautious about interpreting AMIE potentials below the transitional latitude, since data coverage is typically sparse there. The equipotential contours (black curves) in Figure 1 can be regarded as contours of constant Hamiltonian (or total energy, kinetic plus potential) per unit charge (in units of keV) for particles with first adiabatic invariant $M = 0$. The plus signs on these contours mark drift-time intervals of equal length as cold plasma would drift from the neutral line along the direction of flow shown by the arrows if the corresponding electric field were frozen in time. We mark 60-minute intervals for the prestorm and recovery phase

examples (Figures 1a and 1d) but 10-min intervals for the main phase examples (Figures 1b and 1c), in which the convection electric field is much stronger. Figure 1 shows that the AMIE equipotentials are not symmetric between day and night. In fact there is no identifiable line of symmetry in Figure 1. The lowest L value on the last open equipotential tends to be reached in the evening quadrant. Moreover, open equipotentials connecting the night side to the morning side in Figure 1 are skewed in a manner similar to what *McIlwain* [1974] found when he constructed a magnetospheric electric field model based on geosynchronous particle injection boundaries observed by the ATS-5 satellite during substorms. Finally, the locations of x-type
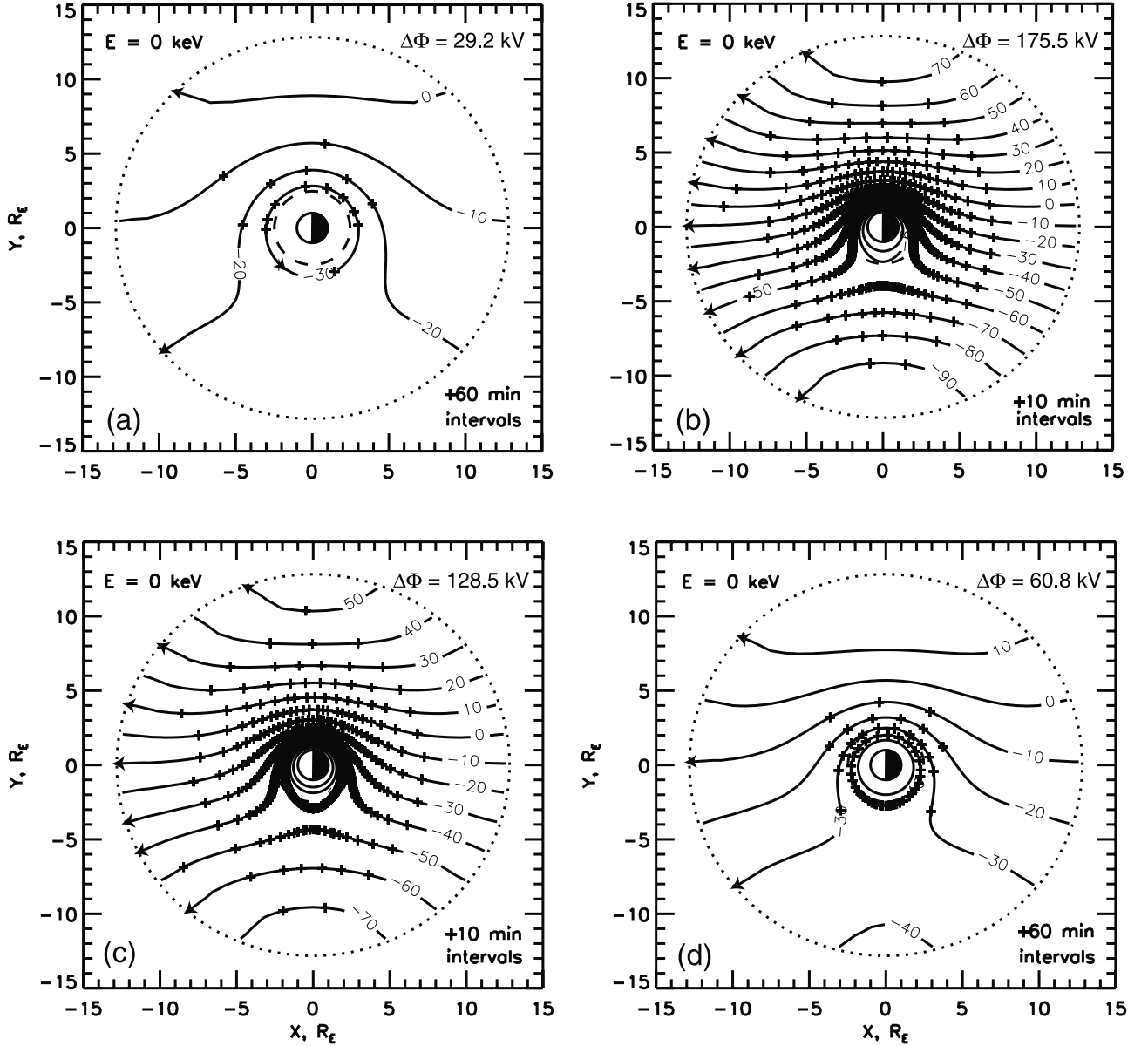
Figure 2. Patterns of equatorial equipotentials in our simplified electric field model for the same total cross polar cap potential drops as in the AMIE model for the times in Figure 1: (a) 29.2 kV, (b) 175.5 kV, (c) 128.5 kV, and (d) 60.8 kV.

stagnation points (i.e., their values of L and MLT) in the quasi-static cold plasma flow patterns illustrated in Figure 1 vary with time.

[15] For comparison with the AMIE-based equipotential patterns shown in Figure 1, each panel in Figure 2 shows equatorial equipotential contours of the combined potential function (corotation plus convection) based on the "simplified" convection electric field model defined by equation (8). For fairness we require the simplified model to impose the same total potential drop across the polar cap as the AMIE potential function provides at the corresponding time for each panel in Figure 1. For example, since AMIE imposed a total cross polar cap potential drop of 29.2 kV at 0100 UT on 19 October 1998 (Figure 1a), we assigned 25 kV to the Volland-Stern ($\gamma = 2$) term and 4.2 kV to the Brice-Nishida ($\gamma = 1$) term in equation (8) so as to generate

the equipotential contours plotted in Figure 2a. Unlike AMIE-based patterns, equipotential patterns derived from the simplified model are symmetric about the dawn-dusk meridian. The lowest L value on the last open equipotential contour occurs at dawn in each panel of Figure 2, and the x-type stagnation point for cold plasma flow in the simplified model always occurs at dusk.

[16] The Stern-Volland ($\gamma = 2$) term in equation (8) generates an equatorial electric field of strength $|\nabla\Phi_{\text{simple}}| = 0$ at $r = 0$, of strength $|\nabla\Phi_{\text{simple}}| = (V_0/2b)|\cos\phi| \approx 0.153|\cos\phi|$ mV/m at the neutral line ($r = b$), and of maximum strength $|\nabla\Phi_{\text{simple}}| \approx 0.88(V_0/b) \approx 0.27$ mV/m at $r \approx 0.54b \approx 6.93\ R_E$, $\phi = \pm\pi/2$ (i.e., on the dawn-dusk meridian). The Brice-Nishida ($\gamma = 1$) term in equation (8) generates an equatorial electric field of strength $|\nabla\Phi_{\text{simple}}| = (1/2b)|\cos\phi|\Delta V(t)$ at the neutral line ($r = b$) and of
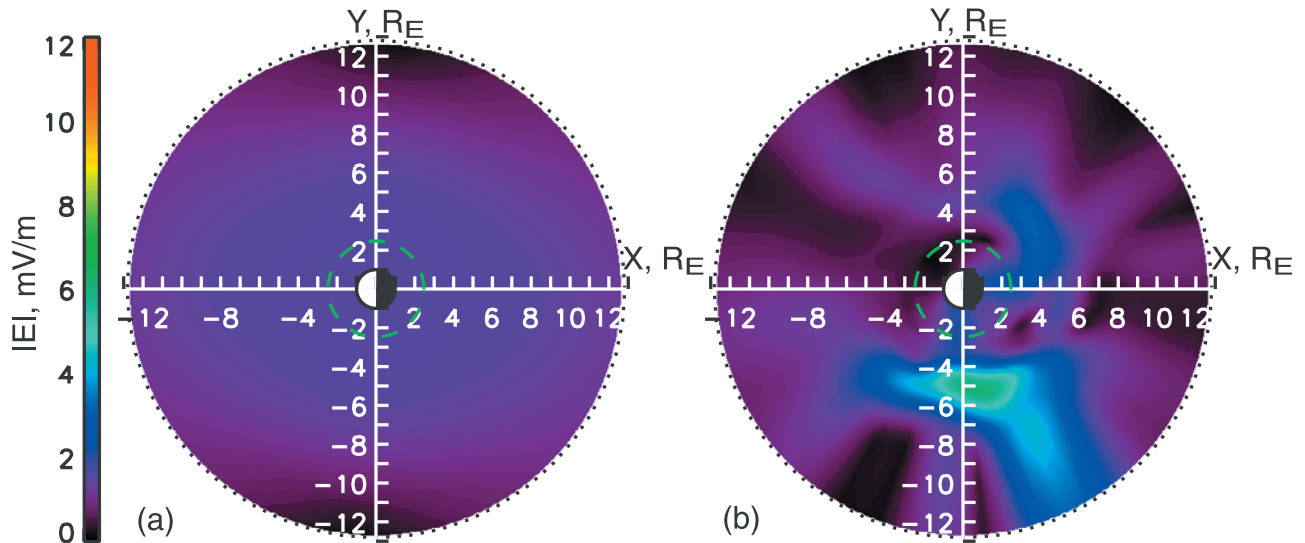
Figure 3.   The equatorial electric field intensity $|E|$ in mV/m in the Earth's corotating frame for (a) the simplified electric field model for a cross polar cap potential drop of 175.5 kV which is the same total AMIE cross polar cap potential drop at 0800 UT on 19 October 1998, and (b) 0800 UT on 19 October 1998 using AMIE potentials. The green dashed curve at 2.54 R_E maps to the AMIE transitional latitude of 50° in our magnetic field model.

maximum strength $|\nabla\Phi_{\text{simple}}| = (3/4b)\Delta V(t)$ at $r = 0$. These last two expressions amount to $0.612|\cos\ \phi|$ mV/m and 0.918 mV/m, respectively, if (for example) $\Delta V(t) = 100$ kV. (The equatorial electric field for $\gamma = 1$ is not strictly uniform in Dungey's model magnetosphere, but the maximum in $|\nabla\Phi_{\text{simple}}|$ at $r = 0$ broadly spans the quasi-dipolar region.) Although $\nabla\Phi_{\text{simple}}$ remains algebraically simple even if both terms ($\gamma = 2$ and $\gamma = 1$) are included together in equation (8), it is more cumbersome to locate maxima in

$|\nabla\Phi_{\text{simple}}|$ in this case. However, it stands to reason that maxima in $|\nabla\Phi_{\text{simple}}|$ with both terms present would exceed (and be located somewhere between) maxima in $|\nabla\Phi_{\text{simple}}|$ with either term neglected. Figure 3a shows an example of the equatorial electric field intensity $|E| = |\nabla\Phi_E|)$ in the Earth's corotating frame in the simplified model for a total cross polar cap potential drop of 175.5 kV, which corresponds to the total AMIE polar cap potential drop for 0800 UT on 19 October 1998. There is day-night symmetry in $|E|$
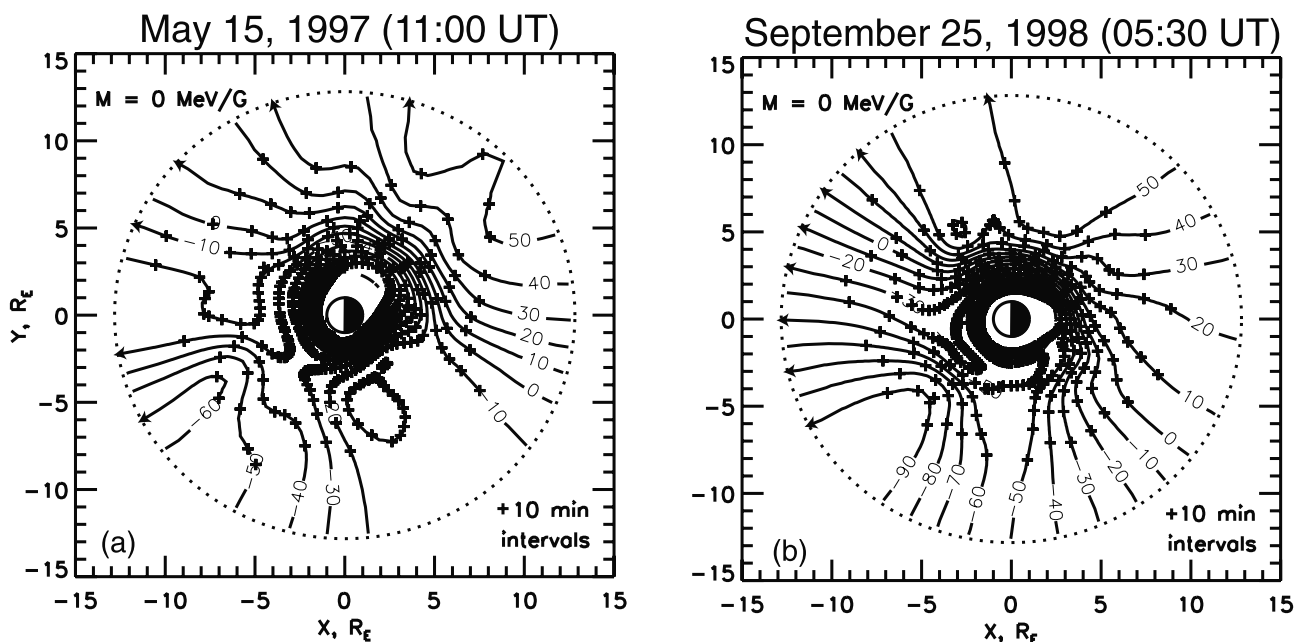

Figure 4.   Patterns of equatorial AMIE plus cororation equipotentials are shown for (a) 1100 UT of the 15 May 1997 storm and (b) 0530 UT of the 25 September 1998 storm. These two times correspond to the storm main phases.

in the simplified model. For this particular example, the maximum $|E|$ (=1.5 mV/m) is attained at 3.5 R_E at dusk and at dawn.

[17] During storm main phases, the equatorially mapped AMIE convection electric field tends to have a much stronger (and more narrowly confined) interior maximum in $|\nabla\Phi_E|$ than the simplified model has. This feature is consistent with radar [*Yeh et al.*, 1991] and satellite [*Rowland and Wygant*, 1998; *Anderson et al.*, 2001] observations. Indeed, the region of strongest AMIE electric field is often concentrated in a particular sector of MLT. During the early main phase (0800 UT) of the 19 October 1998 storm (see Figure 1b and Figure 3b) the electric field was strongest in the evening sector. Figure 3b shows the equatorial AMIE electric field intensity $|E|$ in the Earth's corotating frame for 0800 UT on 19 October 1998. The AMIE electric field is quite strong on the dusk side at $L \sim 3–7$, as well as in the evening sector at $L \gtrsim 4$. The maximum $|E|$ (= 6.1 mV/m) is attained on the duskside at $L = 5.3$. *Wygant et al.* [1998] showed from CRRES observations that the electric field can reach values of 6 mV/m between $L = 2$ and $L = 5$ on the dusk side during the main phase of very intense storms. Thus the AMIE electric field intensity during the main phase of the 19 October 1998 storm is consistent with the findings of *Wygant et al.* [1998]. Figures 4a and 4b show examples of AMIE equipotentials in the equatorial plane during the main phases of the 15 May 1997 and 25 September 1998 storms, respectively. The AMIE electric field was stronger in the morning quadrant than elsewhere at 1100 UT during the main phase of the 15 May 1997 storm (see Figure 5a). The AMIE electric field was strong at low L values ($L < 4$) from premidnight to postdawn at 0530 UT during the main phase of the 25 September 1998 storm (see Figure 5b). For all three storms the equipotentials were skewed so that particles transported closest to Earth would have come primarily from the duskside of the plasma sheet. A concentration of electrostatic field on the nightside is consistent with what is found in self-consistent calculations of electrostatic and induced electric fields in the Rice Convection Model (RCM). *Fok et al.* [2001] reported that the electric field was strongest in the evening quadrant at low L values during an RCM simulation of the 2 May 1986 storm event. We note though that the AMIE electric field is purely electrostatic and the RCM electric field includes an induced electric field.

[18] To illustrate further the variability of equatorial AMIE equipotential patterns, we locate the x-type stagnation point associated with the separatrix between open and closed equipotentials at 5-min intervals during the 3 GEM storms. Stagnation points for general M are identified by finding where the gradient of the Hamiltonian H given by equation (7) is zero: $\partial H/\partial r = (1/r)(\partial H/\partial\phi) = 0$. This part of the procedure is easily automated. Here we treat the case $M = 0$. However, as there may be several stagnation points even for $M = 0$, we distinguish between x-type and o-type stagnation points by examining the equipotential contour through each stagnation point. When there is more than one x-type stagnation point, we choose the one with the lowest L value on a drift separatrix that resembles an open-closed equipotential boundary.

[19] The top two panels of Figure 6 show the equatorial radial distance R_0 (in units of Earth radii) to, and the MLT of,
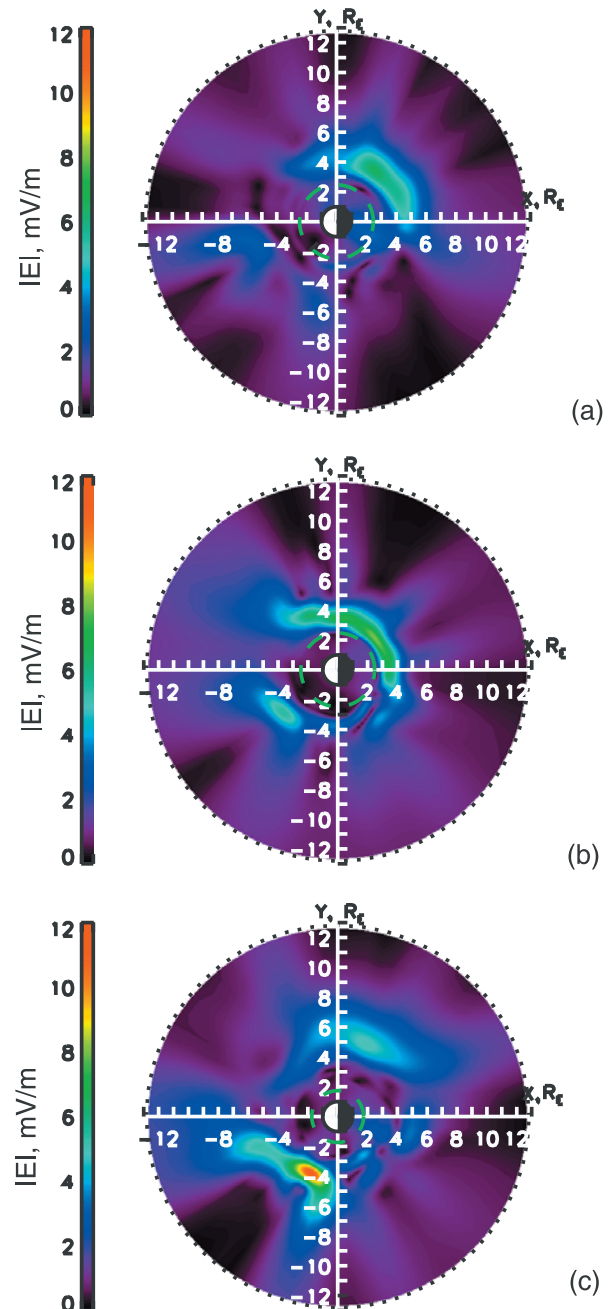

Figure 5. The equatorial electric field intensity $|E|$ in mV/M in the Earth's corotating frame for (a) 1100 UT on 25 May 1997, (b) 0530 UT on 25 September 1998, and (c) 2100 UT on 15 July 2002 using AMIE potentials. In Figure 5c the green dashed curve at 1.74 R_E maps to the AMIE transitional latitude of 40° in our magnetic field model.

each thus chosen x-type stagnation point during the 18–21 October 1998 storm. The cross symbols correspond to AMIE x-type stagnation points, while the filled circles correspond to the x-type stagnation points in the simplified electric field model with the same (as AMIE) total cross polar cap potential drop (shown in the third panel of Figure 6). The equatorial radial distance to the x-type stagnation point in the simplified model tends to track that found in the AMIE
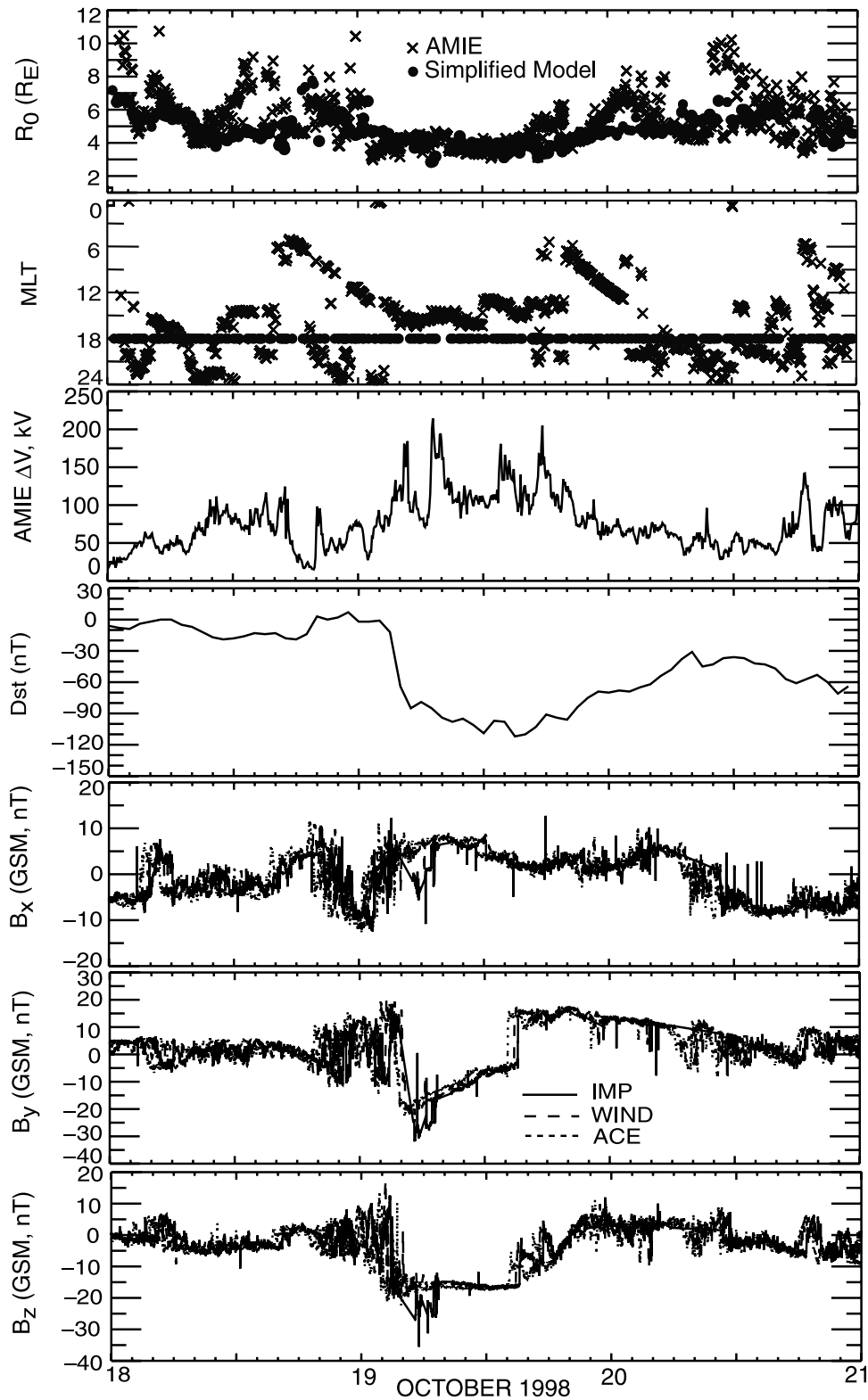
Figure 6. The top panel shows the equatorial radial distance in Earth radii to the x-type stagnation point in the AMIE model (cross signs) and in the simplified model (filled circles) during 18–21 October 1998. The second panel shows the magnetic local time (MLT) of the x-type stagnation point in the AMIE model (cross signs) and simplified model (filled circles) at the same times. The third through seventh panels show time traces of the total AMIE cross polar cap potential drop, the *Dst* index, and the GSM x-, y-, and z-components of the interplanetary magnetic field, respectively. The location of the satellites in GSE coordinates were ACE (230, −38, −6) R_E, WIND (95, 33, 6) R_E, and IMP (20, −23, −25) R_E.
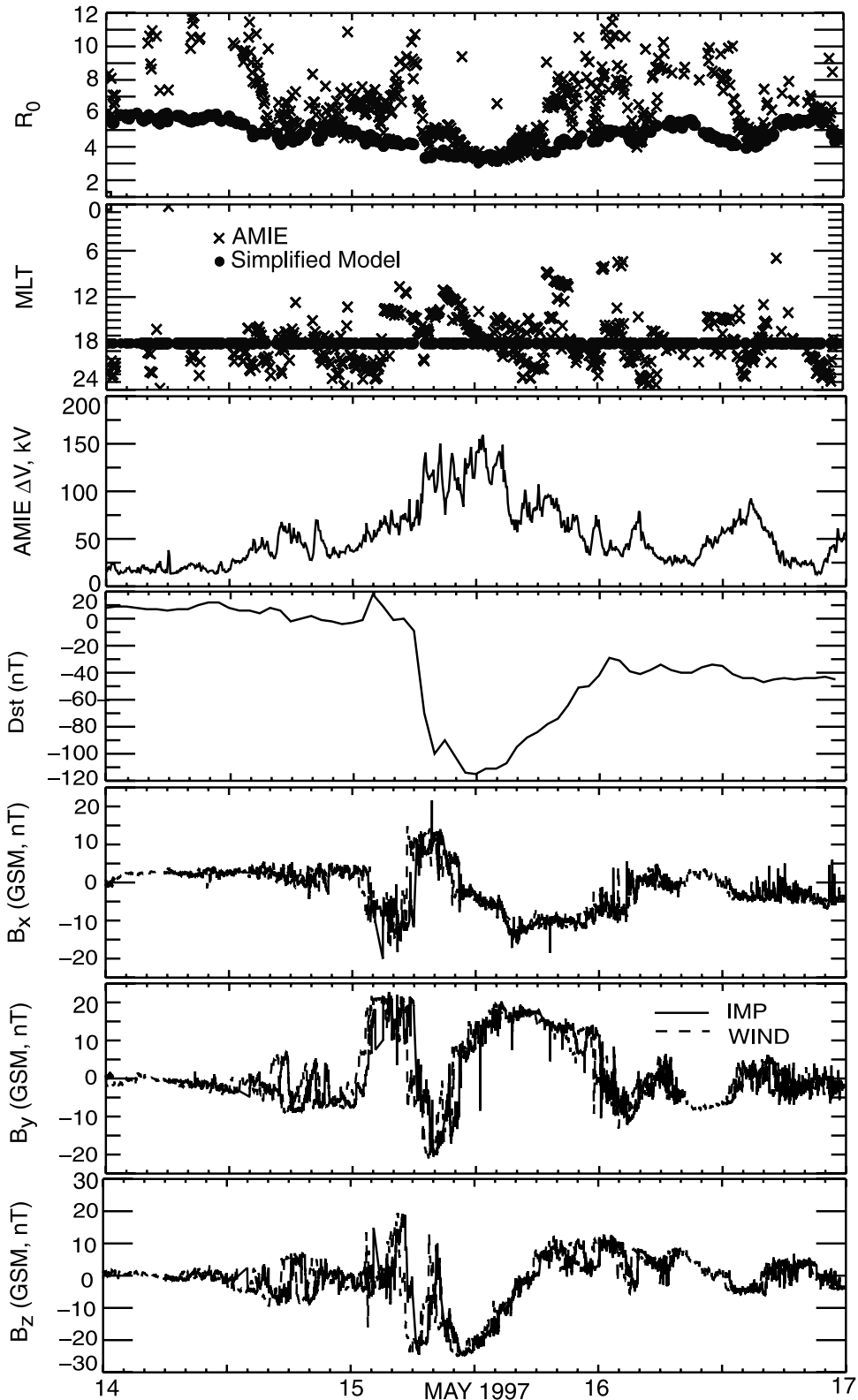
Figure 7. Same data format as in Figure 4, but for 24–27 September 1998. The location of the satellites in GSE coordinates were ACE (241,−31,13) R_E, WIND (183, 15, −6) R_E, and IMP (25, −19, −26) R_E.

model. This is not surprising, since the same total cross polar cap potential drop deduced from AMIE was also used in the simplified model. MLT values of AMIE stagnation points are quite variable, however, whereas MLT values of

stagnation points in the simplified model are fixed at 1800 (dusk).

[20]   To relate the locations of x-type stagnation points to phases of the storm, we show the *Dst* trace in the fourth
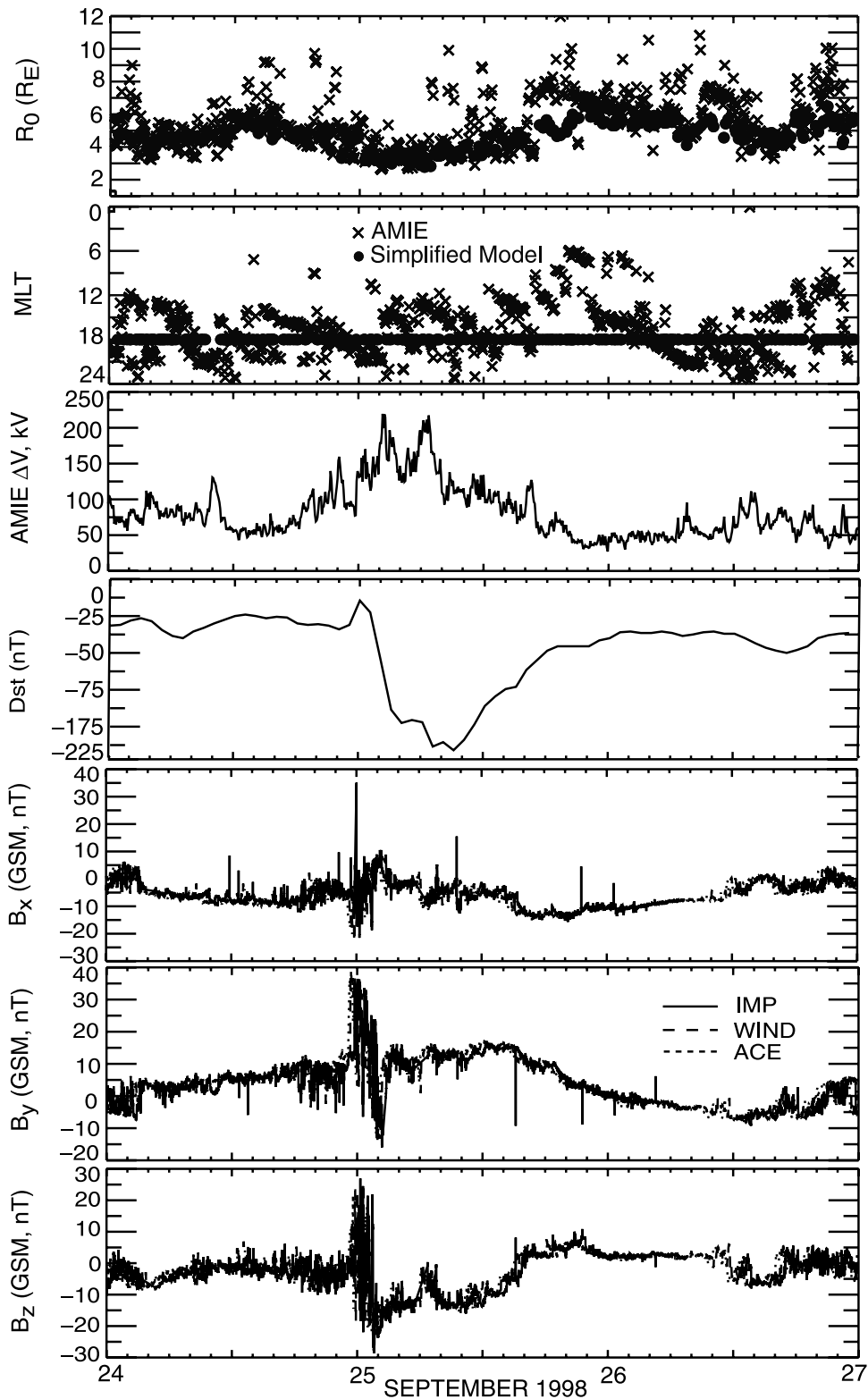
Figure 8. Same data format as in Figure 4, but for 14–17 May 1997. The location of the satellites in GSE coordinates were WIND (191, 3, 18) R_E, and IMP (30, 21, −5) R_E.

panel of Figure 6. Traces of the x, y, and z components of the interplanetary magnetic field measured by the IMP (solid curve), WIND (long dashed curve), and ACE (short dashed curve) satellites are shown respectively in the fifth

through seventh panels of Figure 6. The storm main phase occurred from 0400 UT to 1700 UT on 19 October 1998, during which time the equatorial radial distance to the x-type stagnation point in both models (AMIE and simpli-
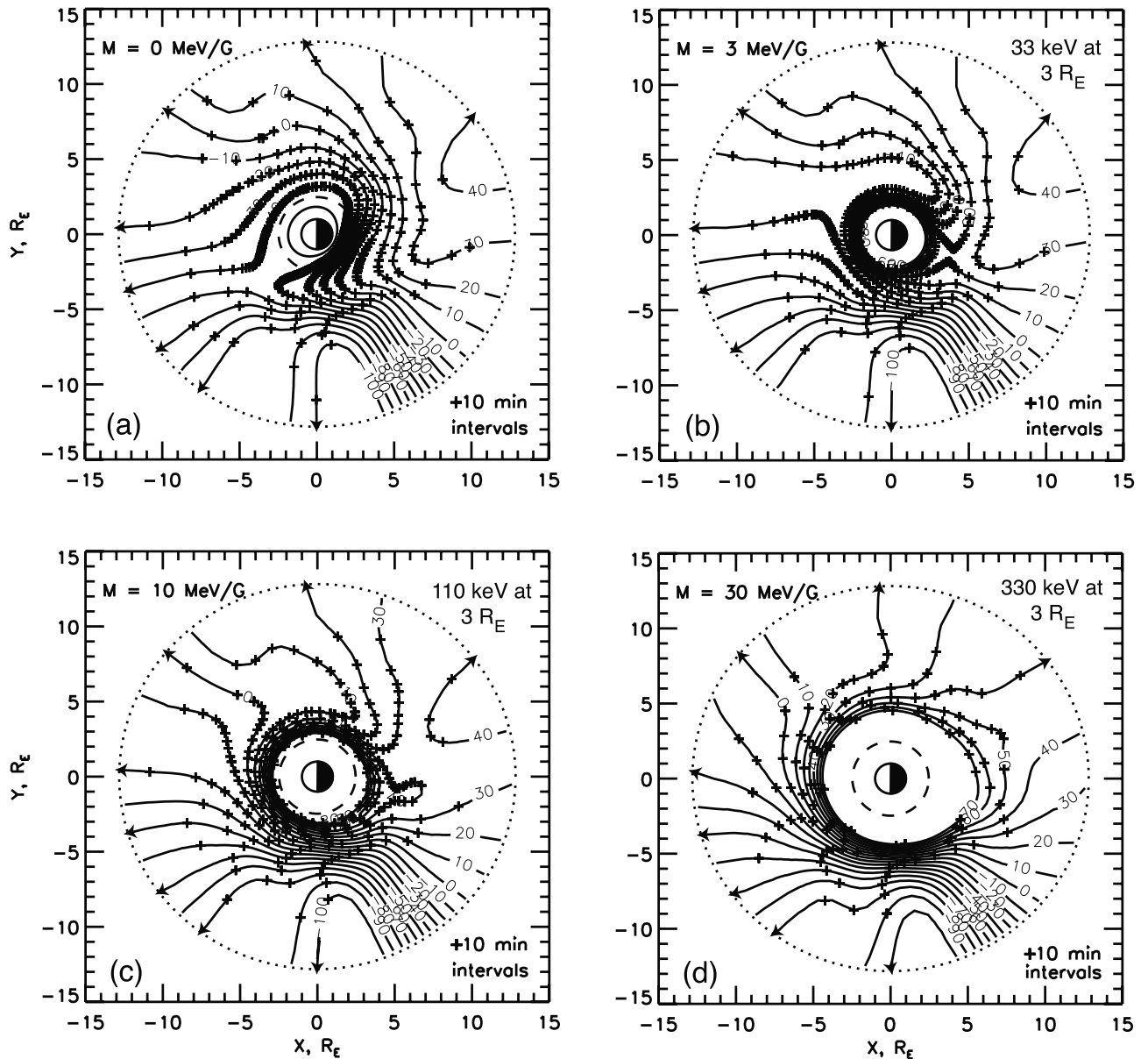
Figure 9. Equatorial quasi-drift paths of singly-charged ions with $M =$ (a) 0, (b) 3 MeV/G, (c) 10 MeV/G, and (d) 30 MeV/G in snapshot of AMIE electric field model for 0800 UT on 19 October 1998. The black curves are contours of constant Hamiltonian per unit charge.

fied) was smallest, as expected. During the storm main phase, when the z-component of the interplanetary magnetic field was negative and relatively steady, the x-type stagnation point was located mainly in the afternoon quadrant (see Figure 6, second panel). The longitude of the x-type stagnation point during the main phases of the 15 May 1997 storm (see Figure 7) and of the 25 September 1998 storm (see Figure 8) also occurred predominantly in the afternoon quadrant. This seems to be a typical feature of AMIE equipotentials.

5. Ion and Electron Quasi-Drift Paths

[21] When mapped to the equatorial plane, the stormtime AMIE convection electric field tends to be concentrated (especially during main phase) in a rather narrow sector ($\sim$60° wide) of nightside MLT and tends to reach a pronounced maximum at $L \sim 2-5$ within that sector. (The MLT location on which the favored sector is centered can be quite variable.) These tendencies remain noticeable in Figures 3a and 5. In this section we compare the effects of AMIE and simplified electric field models on the drift motions of particles with $M = 0$, 3, 10, and 30 MeV/G, which correspond to ion kinetic energies $E = 0$, 33, 110, and 330 keV at $r_0 = 3$ R_E. Our results are shown below in figure panels labeled (a)–(d), respectively. Values of $M = 3$ and 10 MeV/G largely span the range of representative ring-current energies, whereas $M = 30$ MeV/G seems more representative of an ionic radiation belt. Here the drift paths are calculated under both the time-independent AMIE
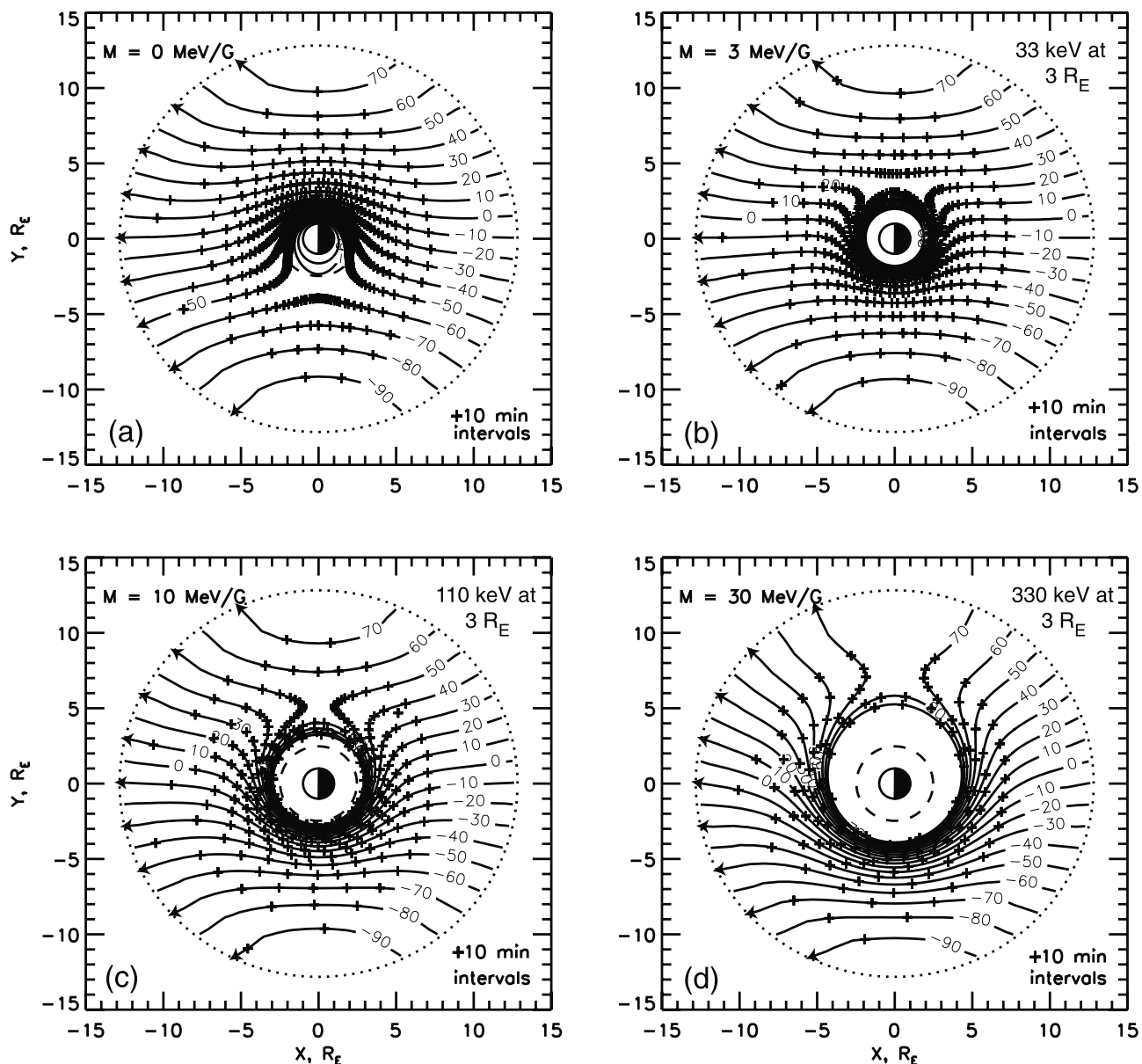
Figure 10. Equatorial quasi-drift paths of singly charged ions with M = (a) 0, (b) 3 MeV/G, (c) 10 MeV/G, and (d) 30 MeV/G in our simplified electric field model for a cross polar cap potential drop of 175.5 kV, same total AMIE cross polar cap potential drop at 0800 UT on 19 October 1998.

electric field model and the time-independent simplified electric field model (with the same potential drop across the polar cap) for selected times of interest during the storms of 19 October 1998 and 15 July 2000. As we have said, the purpose of the present study is to set the stage for realistic simulations with time-dependent electric fields by gaining an appreciation for the characteristics of quasi-steady state drift paths for $M \geq 0$, calculated as if the electric fields were frozen in time.

5.1. Quasi-Drifts During Large Storm of 19 October 1998

[22] We calculate the quasi-steady state drift paths of equatorially mirroring (i.e., with second invariant $J = 0$) singly charged ions with constant first invariant M, using

the Hamiltonian given by equation (7). Figure 9 shows representative results obtained by using the AMIE electric field model for 0800 UT (early main phase) during the 19 October 1998 storm. For ions with M = 3, 10, and 30 MeV/G (Figures 7b, 7c, and 7d) the x-type stagnation point in the drift at 0800 UT (early main phase) on 19 October 1998 occurs within a few hours of midnight. Ions with lower M values can penetrate deeper into the magnetosphere on the dusk side than ions with higher M values, for which azimuthal $\mathbf{B} \times \nabla B$ drifts compete more effectively with radial and azimuthal $\mathbf{E} \times \mathbf{B}$ drifts in determining the trajectories. Because of the strong electric field in the evening sector at this time, there was rapid transport (requiring only $\sim$20$-$30 min) of ions with M values representative of the ring current from the neutral
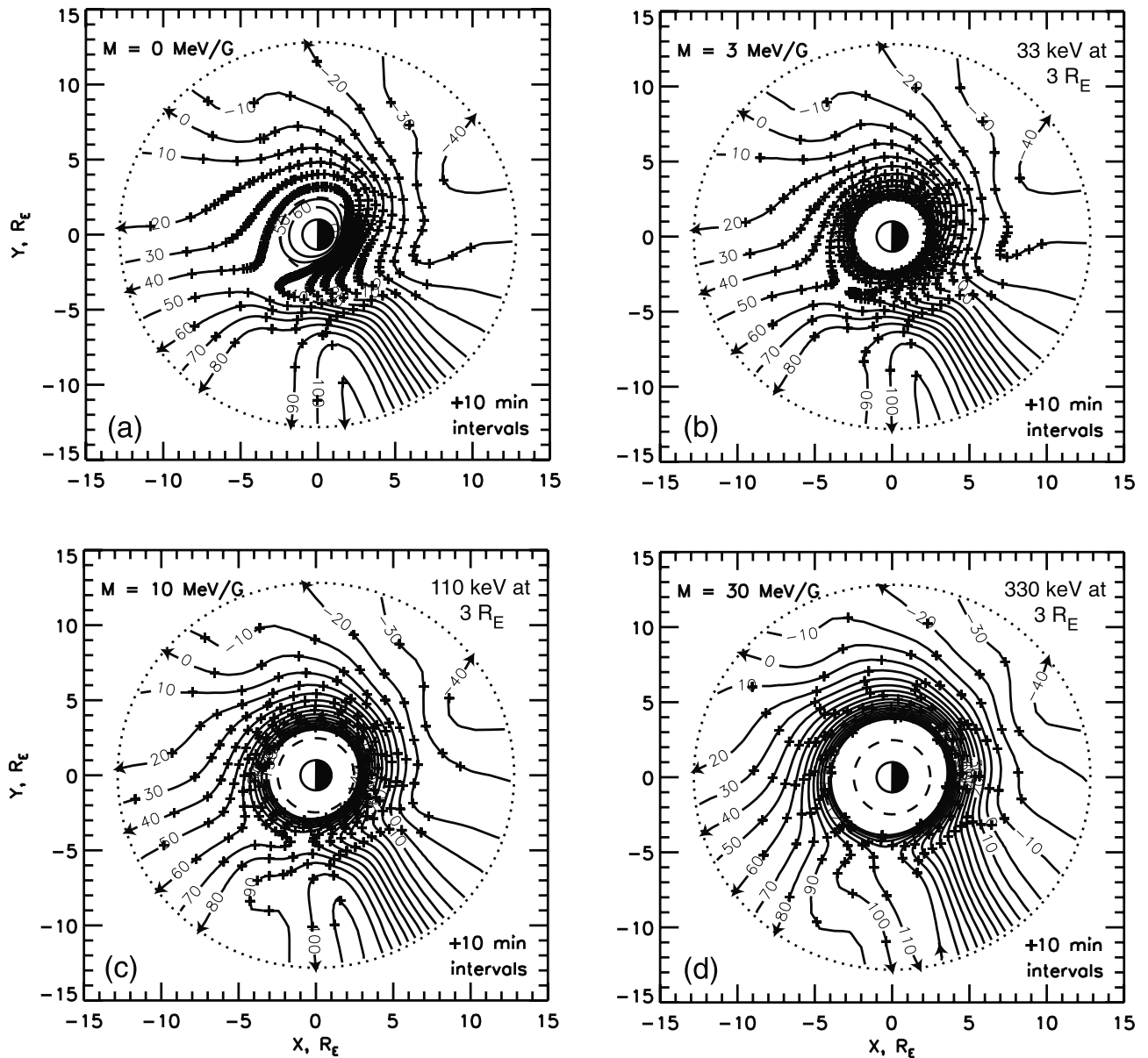
Figure 11.   Equatorial quasi-drift paths of electrons with M = (a) 0, (b) 3 MeV/G, (c) 10 MeV/G, and (d) 30 MeV/G in snapshot of AMIE electric field model for 0800 UT on 19 October 1998.

line to $L \sim 2–5$ near dusk, where the partial ring current typically resides. Mid-latitude magnetometer data [*Clauer et al.*, 2003] confirm that such an asymmetric ring current formed about 20 min after a strongly southward B_z occurred on 19 October 1998. Thus, an AMIE-based electric field model can account for the observed rapid development of an asymmetric ring current during the 19 October 1998 storm.

[23]   For comparison with the AMIE ion drift paths shown in Figure 9, drift paths of ions with M = 0, 3, 10, and 30 MeV/G in the simplified electric field model (with the same total potential drop of 175.5 kV across the polar cap) are shown in Figure 10. The x-type stagnation points in the drift of ions with M = 3, 10, and 30 MeV/G occur at dawn in the simplified model. The drift time of 3 MeV/G ions from the neutral line to $L \sim 4$ at dusk (where the partial ring current forms) in the simplified model requires about

1.5 hours, which is significantly longer than in the AMIE electric field model ($\sim$20 min.), as well as significantly longer than the formation time of the partial ring current as observed by *Clauer et al.* [2003]. The drift times can be inferred from Figures 9 and 10 by counting the plus signs that mark 10-min intervals.

[24]   *Kistler and Larson* [2000] calculated quasi-steady drift paths of ions using the IMF-dependent *Weimer* [1996] electric field. They considered $B_z = -10$ nT, a solar wind speed of 445 km/s and no dipole tilt as parameters for the *Weimer* [1996] model. These conditions are different than those of the 19 October 1998 storm (see IMF data in Figure 6) in which $B_z \sim -20$ nT during the storm main phase. One of their examples of drift trajectories for 3 MeV/G ions (10 keV at 4.5 R_E for 08:00 MLT; see left panel of second row of Figure 5a of *Kistler and Larson* [2000]) shows a stagnation point in the ion drift at $\sim$4 R_E
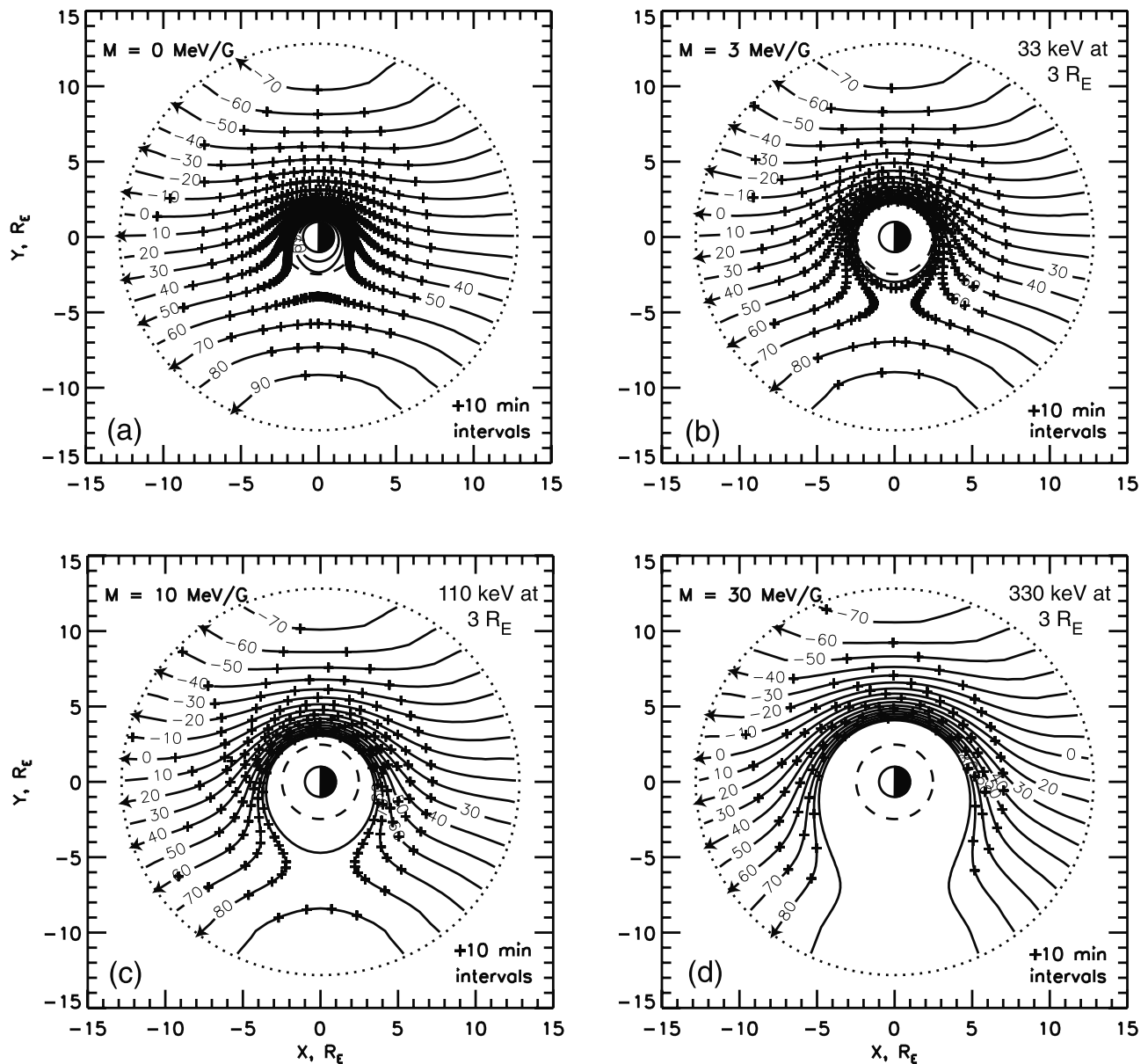
Figure 12. Equatorial quasi-drift paths of electrons with M = (a) 0, (b) 3 MeV/G, (c) 10 MeV/G, and (d) 30 MeV/G for a cross polar cap potential drop of 175.5 kV, same as total AMIE cross polar cap potential drop at 0800 UT on 19 October 1998.

around 2000 MLT. This is near the AMIE stagnation point of ions (≈ 4 R_E at 2245 MLT) for 0800 UT on 19 October 1998. Thus the ion stagnation points in the *Weimer* [1996] and AMIE models are not too far apart even for somewhat different IMF conditions.

[25] We have also calculated quasi-drift trajectories of equatorially mirroring ($J = 0$) electrons from the Hamiltonian function specified by equation (7). Figure 11 shows quasi-drift paths of electrons with M = 0, 3, 10, and 30 MeV/G in the quasi-steady AMIE electric field model for 0800 UT (early main phase) during the 19 October 1998 storm. The x-type stagnation points in the drift of electrons with M = 3, 10, and 30 MeV/G are located within 3 hours MLT of dusk. As we found for ions with M values corresponding to ring current energies, electrons with M = 3 and 10 MeV/G would have had rapid access (requiring only $\sim$20 min) from the

neutral line toward L values where the partial ring current formed near dusk. However, unlike ions of similar M, a significant fraction of electrons are diverted toward morning in this field model.

[26] For comparison with the AMIE-based electron trajectories in Figure 11, quasi-drift paths of electrons with M = 0, 3, 10, and 30 MeV/G in the simplified electric field model are shown in Figure 12. The x-type stagnation points in these electron drift patterns occur at dusk. Moreover, electrons with M = 3, 10, and 30 MeV/G tend to not penetrate as deeply in L on the evening side in the quasi-steady simplified model as they do in the quasi-steady AMIE electric field model for this time during the storm.

[27] Thus far we have shown some examples of particle quasi-drift trajectories to illustrate important differences between drift characteristics in the AMIE and simplified
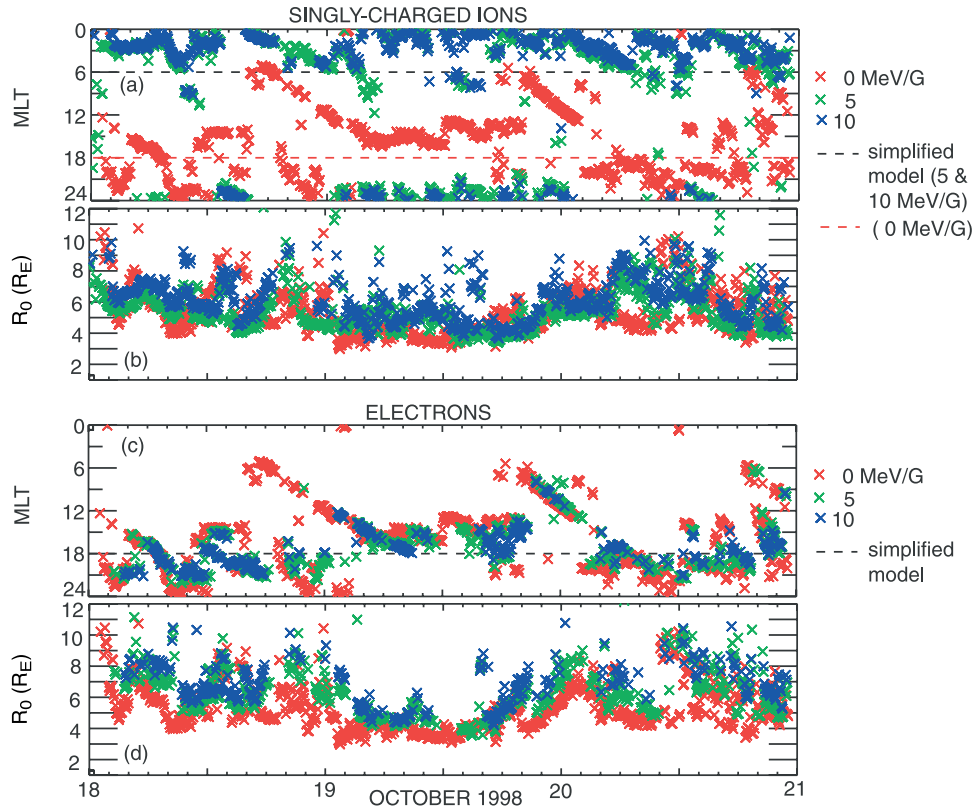
Figure 13. MLT and equatorial radial distance R_0 of the x-type stagnation points in drift of singly-charged ions and electrons in AMIE electric field model during 18−21 October 1998. The cross signs correspond to particles with $M = 0$ (red), 5 MeV/G (green) and 10 MeV/G (blue) in the AMIE model. The dashed curves correspond to the simplified electric field model.

electric field models during the early main phase of a large storm. Particle quasi-drift patterns in fact vary (along with the AMIE model field) throughout a storm. To illustrate this variability we show in Figure 13 the locations of x-type stagnation points in the drift of equatorially mirroring ions and electrons with representative values of M during the prestorm, main, and recovery phases of the 19 October 1998 storm. Red, green, and blue cross symbols correspond to the AMIE stagnation points for ions with M values of 0, 5, and 10 MeV/G, respectively. Figure 13a shows the MLT of the x-type stagnation points of singly-charged ions during 18−21 October 1998. The locations of stagnation points for zero-energy ($M = 0$) ions or electrons were already presented in Figure 6 and discussed in the section on equipotentials; the results are shown again here for comparison with $M = 5$ and 10 MeV/G. The AMIE x-type stagnation points of ions with 5 and 10 MeV/G occurred mostly between evening and dawn (∼2100 to 0600 MLT) during the entire time period shown. During the main phase of the storm (0400 UT-1700 UT) on 19 October 1998, they occurred mostly within 3 hours of midnight. In contrast the x-type stagnation points of ions with $M = 5$ and 10 MeV/G in the simplified electric field model always occur at dawn. Figure 13b shows the equatorial radial distance R_0 to the x-type stagnation points for ions in the AMIE field model. At any given time, the distance to the x-type stagnation point tends to be larger for ions with a larger first invariant.

[28] Figure 13c shows the MLTs of x-type stagnation points for electrons with the same three M values during 18−21 October 1998. The x-type stagnation points of electrons with $M = 5$ and 10 MeV/G occur mainly between dawn and evening (0600 to 2100 MLT) during the entire time period. During the main phase of the storm, the x-type stagnation points of electrons with $M = 5$ and 10 MeV/G occur predominantly in the afternoon quadrant. The electron x-type stagnation point in the simplified model always occurs at dusk (dashed black line).

[29] The most rapid transport of particles occurs where the electric field is strongest. Although we do not show examples of ion drift paths for the two other GEM storms, we find rapid transport of ions with 3 MeV/G from the nightside neutral line to $L \sim 5$ to the morning (∼40 min. to $L \sim 5$ at 0300 MLT) during the main phase (1100 UT) of the 15 May 1997 storm. The most negative Dst of that storm is attained near 1100 UT. At that time the AMIE electric field is strongest in the morning sector at $L \sim 4−6$ as can be seen in either Figure 4a or Figure 5a. It requires about 1 hour for ions with 3 MeV/G to be transported to $L \sim 4$ at ∼2100 MLT from the nightside neutral line during the main phase (0530 UT) of the 25 September 1998 storm. The 0530 UT time is near the most negative Dst of that storm. The corresponding AMIE electric field is strongest at $L \sim 3−4$ from the evening to beyond dawn (see Figures 4b and 5b). We find that the AMIE electric field tends to be strongest in some sector on the nightside. This concen-
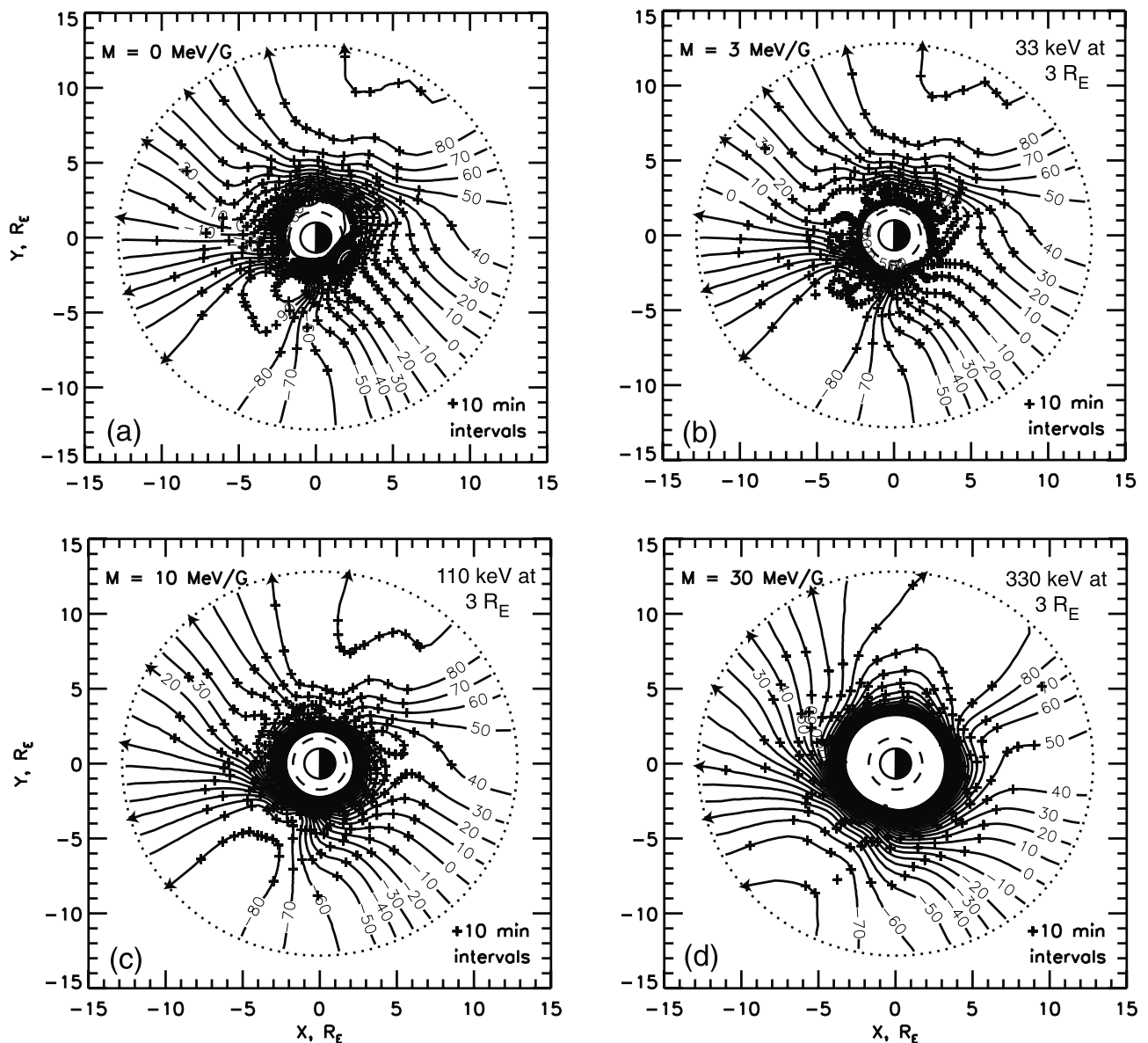
Figure 14. Equatorial quasi-drift paths of singly-charged ions with M = (a) 0, (b) 3 MeV/G, (c) 10 MeV/G, and (d) 30 MeV/G in snapshot of AMIE electric field model for 2100 UT on 15 July 2000. The dashed curve at 1.74 R_E maps to the AMIE transitional latitude 40° in our magnetic field model.

tration of electric field would lead to relatively fast transport there.

[30] In future work we will proceed beyond the present study of quasi-steady drift paths and employ the time-dependent Hamiltonian function specified by equation (7) to simulate the bounce-averaged drift of representative ions and electrons along.

5.2. Quasi-Drifts During the Extremely Large "Bastille Day" Storm of 15−16 July 2000

[31] Ions with M values representative of the ring current population had rapid access from the plasma sheet to the dusk side at $L \sim 3-4$ in the AMIE electric field model during early main phase of the large 19 October 1998 storm.

[32] Next we investigate the particle drifts in the AMIE electric field model during the extremely large 15−16 July 2000 "Bastille Day" storm, in which a minimum Dst of −300 nT was attained. For the main phase of the Bastille Day storm we have needed to extend the AMIE model to lower latitudes than usual so as to account for the detection of large electric fields even at L = 1.5 through DMSP satellite measurements of very large westward ion drifts as low as 35° latitude in the ionosphere at about the time when Dst reached its most negative value (P. C. Anderson, private communication, 2001). In order to accommodate these low-latitude DMSP measurements (along with the usual magnetometer data) in our special AMIE run for the Bastille Day storm, we changed the AMIE transitional colatitude θ_0 in equation (2) from the usual 40° to 50°.

[33] Figure 5c shows the equatorial AMIE electric field intensity in the Earth's corotating frame for 2100 UT for the 15 July 2000 storm. The time of 2100 UT was during the
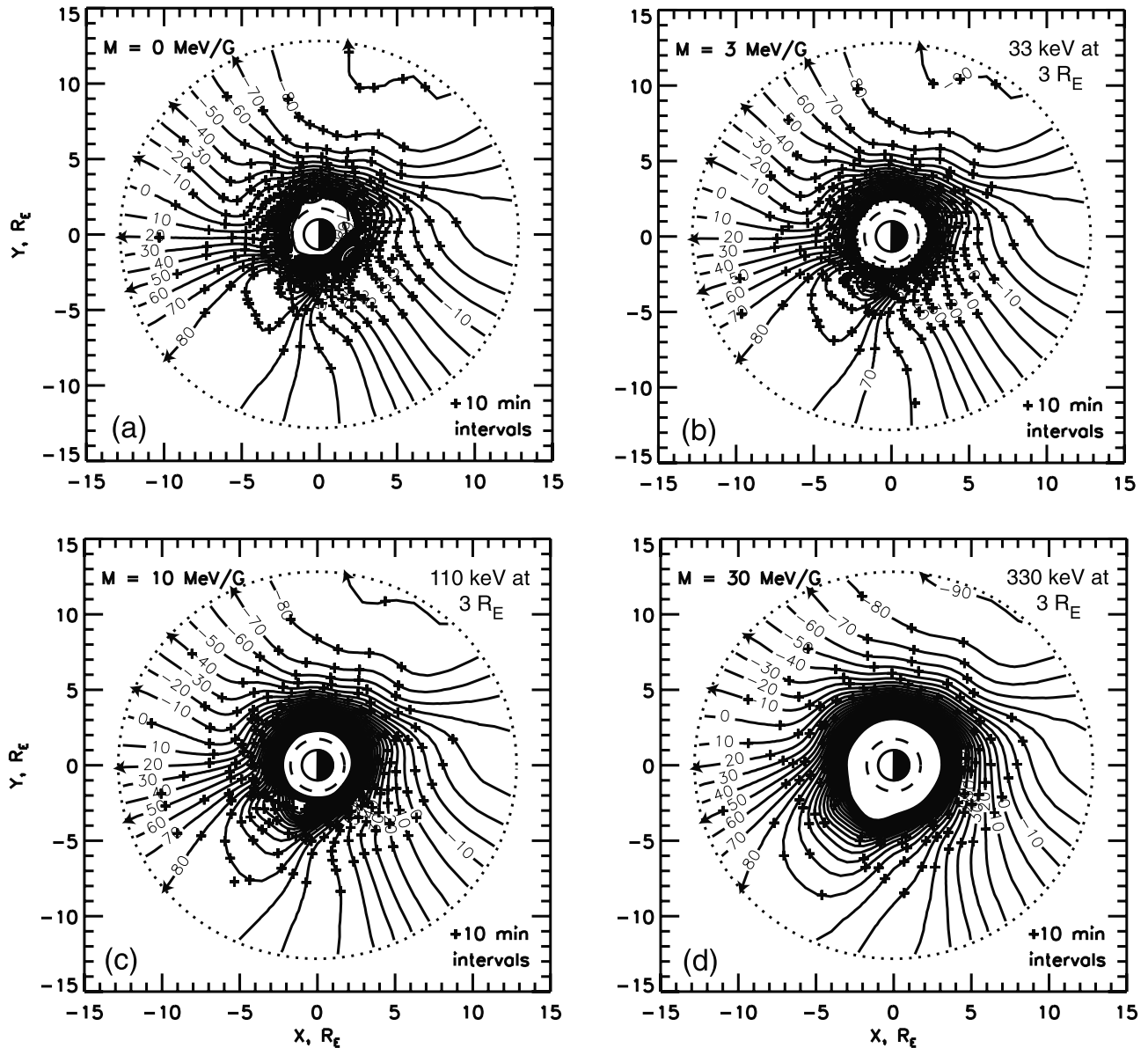
Figure 15. Equatorial quasi-drift paths of electrons with $M =$ (a) 0, (b) 3 MeV/G, (c) 10 MeV/G, and (d) 30 MeV/G in snapshot of AMIE electric field model for 2100 UT on 15 July 2000.

main phase of that storm. Very large electric field intensities ($\sim$5 mV/m) occur as low as $L \sim 2$ near pre-midnight. The AMIE electric field intensity is as large as $\sim$11 mV/m at $L \sim 4$ at predusk.

[34] Figure 14 shows equatorial quasi-drift paths for ions with $M = 0$, 3, 10, and 30 MeV/G at 2100 UT on 15 July 2000. The dashed circle at 1.74 R_E maps to 40° ionospheric latitude ($\theta_0 = 50°$) in our magnetic field model. Values of $M \sim 1-15$ MeV/G are representative of ring current ions. Ions with $M = 3$ MeV/G have access to as low as $L \sim 2$ on the dusk side (see Figure 14b) after about 1.5 hour drift time from the nightside neutral line. Ions with somewhat higher M value (10 MeV/G) have access to as low as $L \sim 3$ in the evening quadrant (see Figure 14c) after drift times $\sim$1 hour. This very deep penetration of ring current ions is consistent with the very strong ring current that was observed during this storm. The total AMIE cross polar cap potential was

166 kV at 2100 UT on 15 July 2000. In the simplified electric field model with the same 166-kV potential drop across the polar cap, ions with $M = 3$ MeV/G have access to as low as $L \sim 2-2.25$ near dusk. However, the corresponding drift times ($\sim$2−3 hours) to such low L values are significantly longer than in the AMIE electric field model. Ions with $M = 10$ MeV/G do not reach $L \sim 3$ in the simplified electric field model, and they require drift times $\sim$1.5 hours even to reach $L \sim 3.5$.

[35] Equatorial quasi-drift paths for electrons with $M = 0$, 3, 10, and 30 MeV/G at 2100 UT on 15 July 2000 are shown in Figure 15. Like the ions with M values representative of the ring current, electrons with $M = 3$ and 10 MeV/G have access to low L values at this time. For a given M value, however, electrons do not have access to as low an L value as ions. Electrons with $M = 3$ MeV/G reach only $L \sim 3$ (see Figure 15b), whereas ions with $M = 3$

MeV/G have access to $L \sim 2$ (see Figure 14b). Electrons with $M = 10$ MeV/G reach only $L \sim 3.5$ (see Figure 15c), whereas ions with $M = 10$ MeV/G have access to $L \sim 2.5$ (see Figure 14c). The drift patterns in Figure 15 also shows that electrons from the evening quadrant of the neutral line tend to be diverted past midnight toward the morning quadrant, whereas corresponding ions in Figure 14 tend to drift past dusk toward the afternoon quadrant.

6. Summary and Conclusions

[36] In this study we have examined inner magnetospheric particle drift characteristics as inferred from quasi-steady realizations of the AMIE electric field in a simple magnetospheric model during four storms. We have chosen to use the AMIE electric field because it includes some important stormtime convection features that have recently been recognized but which have not been included in our previous stormtime simulations. Here we have compared AMIE quasi-drift characteristics with those obtained from the simple semi-empirical model of convection that we have used in previous stormtime simulations. Since stormtime AMIE equipotential patterns are highly variable in time and complicated in spatial structure, the corresponding quasi-drift trajectories are similarly complicated. In contrast, the patterns of equatorial drift trajectories in the simplified model are (by construction) symmetric about the dawn-dusk meridian and mutually similar in shape. AMIE equipotential patterns do, however, show recurrent features that consistently modify particle drift trajectories relative to the simplified model, and these features are important for understanding formation of the stormtime ring current. In particular, during storm main phase the AMIE electric equipotentials tend to be concentrated in a limited MLT sector on the nightside. This concentration leads to rapid inward transport of ions with first invariant values representative of the ring current population from the nightside neutral line to low L values ($\sim 3-4$) near dusk where the partial ring current forms. For example, the transport time from $r_0 = 12.8$ R_E to $r_0 = 3$ R_E for ions with first invariant $M = 3$ (corresponding to kinetic energy $E = 33$ keV at $r_0 = 3$ R_E) or 10 MeV/G (110 keV at $r_0 = 3$ R_E) is on the order of 20 min. Such an access time is consistent with observations [e.g., *Clauer et al.*, 2003] of rapid formation of an asymmetric ring current within half an hour after storm onset. Losses due to charge exchange should be negligible on this time scale. Indeed, *Liemohn et al.* [2001] have found that ion outflow of ions along open drift paths to the dayside magnetopause is the main loss mechanism for the ring current's contribution to *Dst* during the early recovery phase. The same loss process should have been present also during the main phase, when it would have been balanced by access of new ions from the nightside neutral line.

[37] We have investigated particle drifts in the AMIE electric field during the extremely large "Bastille Day" storm of 15 July 2000, when large stormtime penetration electric fields were observed by DSMP satellites (P. C. Anderson, private communication, 2001) to reach to as low as 35° near the time of minimum *Dst* (= −300 nT). Large electric fields at low latitudes of low L values would have lead to a deep penetration of ions with first invariant values

representative of the ring current population during this storm's main phase. Ions with first invariant $M = 3$ MeV/G would have reached $L \sim 2$ about an hour before the first minimum in *Dst* (= nT) was attained at 2130 UT. This deep penetration of ring current ions could account for the very strong ring current that was observed during the "Bastille Day" storm.

[38] In this study we have calculated quasi-steady drift paths in selected "snapshots" of the AMIE electric field. However, time-dependent particle drift equations can be derived easily from the Hamiltonian function specified by equation (7) as a function of M, L, and φ [e.g., *Schulz and Chen*, 1995]. We are currently incorporating the AMIE electric field into truly time-dependent simulations of ring current formation and decay. It will be interesting to see how the more rapid access of ions to the ring current region in consequence of the strength of AMIE electric fields in the evening quadrant of the inner magnetosphere affect the development of the asymmetric and symmetric components of the ring current and the overall ring current energy content.

References

Anderson, P. C., D. L. Carpenter, K. Tsuruda, T. Mukai, and F. J. Rich, Multi-satellite observations of rapid subauroral ion drifts (SAID), *J. Geophys. Res.*, *106*, 29,585–29,600, 2001.

Boonsiriseth, A., R. M. Thorne, G. Lu, V. K. Jordanova, M. F. Thomsen, and D. M. Ober, A semi-empirical equatorial mapping of AMIE convection electric potentials (MACEP) for the January 10, 1997, magnetic storm, *J. Geophys. Res.*, *106*, 12,903–12,917, 2001.

Brice, N. M., Bulk motion of the magnetosphere, *J. Geophys. Res.*, *72*, 5193–5211, 1967.

Chen, A. J., Penetration of low-energy protons deep into the magnetosphere, *J. Geophys. Res.*, *75*, 2458–2467, 1970.

Chen, M. W., and M. Schulz, Simulations of stormtime diffuse aurora with plasmasheet electrons in strong pitch angle diffusion, *J. Geophys. Res.*, *106*, 1873–1886, 2001.

Chen, M. W., M. Schulz, L. R. Lyons, and D. J. Gorney, Stormtime transport of ring current and radiation-belt ions, *J. Geophys. Res.*, *98*, 3835–3849, 1993.

Chen, M. W., M. Schulz, and L. R. Lyons, Simulations of phase space distributions of stormtime proton ring current, *J. Geophys. Res.*, *99*, 5745–5759, 1994.

Chen, M. W., L. R. Lyons, and M. Schulz, Storm-time ring-current formation: A comparison between single- and double-dip model storms with similar transport characteristics, *J. Geophys. Res.*, *105*, 27,755–27,765, 2000.

Clauer, R. C., M. W. Liemohn, J. U. Kozyra, and M. L. Reno, The relationship of storms and substorms determined from mid-latitude ground-based magnetic maps, in *On the Realtionship Between Storms and Substorms*, *Geophys. Monogr. Ser.*, edited by S. Sharma, AGU, Washington, D.C., in press, 2003.

Dungey, J. W., The structure of the exosphere or adventures in velocity space, in *Geophysics, The Earth's Environment*, edited by C. DeWitt,

J. Hieblot, and A. Lebeau, pp. 503–550, Gordon and Breach, London, 1963.

Ebihara, Y., and M. Ejiri, Simulation study on fundamental properties of the storm-time ring current, *J. Geophys. Res.*, *105*, 15,843–15,860, 2000.

Ejiri, M., Trajectory traces of charged particles in the magnetosphere, *J. Geophys. Res.*, *83*, 4798–4810, 1978.

Fok, M.-C., T. E. Moore, J. U. Kozyra, G. C. Ho, and D. C. Hamilton, Three-dimensional ring current decay model, *J. Geophys. Res.*, *100*, 9619–9632, 1995.

Fok, M.-C., R. A. Wolf, R. W. Spiro, and T. E. Moore, Comprehensive computational model of Earth's ring current, *J. Geophys. Res.*, *106*, 8417–8424, 2001.

Jordanova, V. K., J. U. Kozyra, G. V. Khazanov, A. F. Nagy, C. E. Rasmussen, and M.-C. Fok, A bounce-averaged kinetic model of the ring current ion population, *Geophys. Res. Lett.*, *21*, 2785–2788, 1994.

Jordanova, V. K., L. M. Kistler, C. J. Farrugia, and R. B. Torbet, Effects of inner magnetospheric convection on ring current dynamics: March 10–12, 1998, *J. Geophys. Res.*, *106*, 29,705–29,720, 2001.

Kavanagh, L. D., Jr., J. W. Freeman Jr., and A. J. Chen, Plasma flow in the magnetosphere, *J. Geophys. Res.*, *73*, 5511–5519, 1968.

Kistler, L. M., and D. J. Larson, Testing electric and magnetic field models of the storm-time inner magnetosphere, *J. Geophys. Res.*, *105*, 25,211–25,231, 2000.

Liemohn, M. W., J. U. Kozyra, M. F. Thomsen, J. L. Roeder, G. Lu, J. E. Borovsky, and T. E. Cayton, Dominant role of the asymmetric ring current in producing the stormtime *Dst**, *J. Geophys. Res.*, *106*, 10,883–10,904, 2001.

Maynard, N. C., and A. J. Chen, Isolated cold plasma regions: Observations and their relation to possible production mechanisms, *J. Geophys. Res.*, *80*, 1009–1013, 1975.

Maynard, N. C., T. L. Aggson, and J. P. Heppner, The plasmaspheric electric field as measured by ISEE 1, *J. Geophys. Res.*, *88*, 3991–4003, 1983.

McIlwain, C. E., Susbtorm injection boundaries, in *Magnetospheric Physics*, edited by B. M. McCormac, pp. 143–154, D. Reidel, Norwell, Mass., 1974.

Nishida, A., Formation of the plasmapause, or magnetospheric plasma knee, by the combined action of magnetospheric convection and plasma escape from the tail, *J. Geophys. Res.*, *71*, 5669–5679, 1966.

Richmond, A. D., and Y. Kamide, Mapping electrodynamic features of the high-latitude ionosphere from localized observations: Technique, *J. Geophys. Res.*, *93*, 5471–5759, 1988.

Rowland, D. E., and J. R. Wygant, Dependence of the large-scale, inner magnetospheric electric field on geomagnetic activity, *J. Geophys. Res.*, *103*, 14,959–14,964, 1998.

Smith, P. H., N. K. Bewtra, and R. A. Hoffman, Motions of charged particles in the magnetosphere under the influence of a time-varying large scale convection electric field, in *Quantitative Modeling of Magnetospheric Processes, Geophys. Monogr. Ser.*, vol. 21, edited by W. P. Olson, pp. 513–535, AGU, Washington, D.C., 1979.

Stern, D., Models of the Earth's electric field, *NASA/GSFC Rep.*, X-602-74-159, NASA/Goddard Space Flight Cent., Greenbelt, Md., May 1974.

Stern, D. P., Quantitative models of magnetic and electric fields in the magnetosphere, *NASA/GSFC Rep.*, X-602-75-90, NASA/Goddard Space Flight Cent., Greenbelt, Md., April 1975.

Tsyganenko, N. A., Effects of the solar wind conditions on the global magnetospheric configurations as deduced from data-based field models, in *Proceedings of the ICS-3 Conference, Versailles, France, May 12–17, 1996, Eur. Space Agency Spec. Publ.*, ESA SP–389, 181–185, 1996.

Volland, H., A semiempirical model of large-scale magnetospheric electric fields, *J. Geophys. Res.*, *78*, 171–180, 1973.

Volland, H., Models of global electric fields within the magnetosphere, *Ann. Geophys.*, *31*, 154–173, 1975.

Weimer, D. R., Models of high-latitude electric potentials derived with a least error fit of spherical harmonic coefficients, *J. Geophys. Res.*, *100*, 19,595–19,607, 1995.

Weimer, D. R., A flexible, IMF dependent model of high-latitude electric potentials having "space weather" applications, *Geophys. Res. Lett.*, *23*, 2549–2552, 1996.

Wygant, J., D. Rowland, H. Singer, M. Temerin, and M. K. Hudson, Experimental evidence on the role of the large spatial scale electric field in creating the ring current, *J. Geophys. Res.*, *103*, 29,527–29,544, 1998.

Yeh, H.-C., J. C. Foster, F. J. Rich, and W. Swider, Storm time electric field penetration observed at mid-latitude, *J. Geophys. Res.*, *96*, 5707–5721, 1991.

———————————

M. W. Chen, The Aerospace Corporation, MX M2-260, 2350 E. El Segundo Blvd., P. O. Box 92957, Los Angeles, CA 90009-2957, USA. (Margaret.W.Chen@aero.org)

L. R. Lyons, Department of Atmospheric Sciences, University of California, Los Angeles, Los Angeles, CA 90095-1565, USA. (larry@atmos.ucla.edu)

G. Lu, High Altitude Observatory, NCAR, Boulder, CO 80307-3000, USA. (ganglu@hao.ucar.edu)

M. Schulz, Lockheed Martin Advanced Technology Center, Building 255, o/H1-11, 3251 Hanover Street, Palo Alto, CA 94304, USA. (mike.schulz@lmco.com)